International Conference on Renewable Energies and Power Quality (ICREPQ'15)
La Coruña (Spain), 25th to 27th March, 2015
Renewable Energy and Power Quality Journal (RE&PQJ)
ISSN 2172-038 X, No.13, April 2015

Experimental investigation on saturated critical heat flux of refrigerant R134a at high saturation temperatures

F. Botticella[1], F. De Rossi[1], R. Mastrullo[2], G.P. Vanoli[1], L. Viscito[2]

[1] Department of Engineering
Sannio University
Corso Garibaldi 107, Palazzo dell'Aquila Bosco Lucarelli, 82100, Benevento (Italy)

[2] Department of Industrial Engineering
Federico II University of Naples
P.le Tecchio 80, 80125, Naples (Italy)
e-mail: rita.mastrullo@unina.it

Abstract. This article presents saturated critical heat flux results in an aluminium heat sink at high saturation temperatures. The test section is made up of seven rectangular mini-channels that are 1.0 mm deep and 2.0 mm wide, with a heated length of 25 mm. R134a has been used as the working fluid. The effect of mass flux G (ranging from 150 up to 330 kg/m^2 s) has been investigated. All tests have been performed at medium to high saturation temperatures, ranging from 25 °C up to 70 °C. The experimental results showed that the saturation temperature had only a mild influence on the CHF, at each mass flux imposed. On the contrary, when increasing the mass flux at a given saturation temperature, the critical heat flux was observed to increase significantly.
Finally, the prediction capability of a well-known critical heat flux correlation has also been tested.

Key words
Minichannels, chip cooling, concentrated photovoltaic (CPV), R134a, critical heat flux (CHF).

1. Introduction

In the last decades, the size of electronic devices has considerably decreased, and this has made possible to obtain faster chip speeds. At the same time this circumstance has led to greater chip power densities. Consequently, recent progresses in the microelectronics field have resulted in dissipation of much higher heat fluxes than ever before, exceeding the fan cooling forced convection limits. In addition, the new generation of photovoltaic cells attempts to enhance the overall panel power by concentrating always more the solar illumination in small operating spots. This technique requires the cell to be adequately cooled down in order to avoid high working temperatures and therefore a substantial drop in the panel efficiency. Royne et al. [1] stated that for densely packed cells with very high solar concentration (>150 suns), microchannel technology is one of the few feasible cooling solutions, being these heat fluxes behind the limit of air forced convection.

Microchannel geometry increases heat transfer due to small hydraulic diameters, working both on single-phase (water) or two-phase flows (environmental friendly refrigerants). In particular, two-phase flows are necessary at very high heat fluxes to avoid too high pressure drops related to water at high mass fluxes, thanks to the large latent heat of vaporization of the evaporating fluid.
For this reason, scientific literature has risen a great interest towards small size cooling elements, where the heat is dissipated by boiling mechanism, thanks to its high heat transfer rate. Both for macro and minichannels, the highest limit of the heat transfer is related to the so-called "critical heat flux" (CHF). Beyond CHF, the system is subject to a strong deterioration of the heat dissipation capability and also to a potential risk of burn-out damage.
Most of the researches available in literature concentrate their attention on single-phase flows with water or two-phase flows of refrigerants at saturation temperatures ranging from 20 to 50 °C.
Mauro et al. [2] studied saturated critical heat flux of R134a, R236fa and R245fa in a multi-microchannel copper heat sink, formed by 29 parallel channels that were 199 μm wide and 756 μm deep. The parametric effects of mass velocity, saturation temperature and inlet sub-cooling were investigated. The authors found that higher CHFs were obtainable with a split flow system (one inlet – two outlets), providing also a much lower pressure drop.
Lazarek and Black [3] measured critical heat flux for R113 in a round tube with an internal diameter of 0.31 cm and with two different heating lengths. A correlation was developed to predict critical conditions under low reduced pressures.
Wojtan et al. [4] performed a series of tests with refrigerants R134a and R245fa to determine the saturated critical heat flux in 0.5 and 0.8 mm internal diameter tubes with two different heated lengths. Their results

showed a strong dependence of CHF on mass velocity, heated length and microchannel diameter. On the contrary, no influence of liquid sub-cooling was detected. The authors proposed a new correlation for the prediction of CHF during saturated boiling in microchannels.
Tibiriçá et al. [5] compared CHF results of circular tubes using R134a and R245fa against experimental data obtained with flattened tube having the same equivalent internal diameter of 2.2 mm, but different aspect ratios of 1/4, ½, 2 and 4. Their results showed that the critical heat flux was found to be independent on the tube aspect ratio when the same heated length was kept.
Park and Thome [6] tested R134a, R236fa, R245fa CHF in two different multi-microchannels copper heat sinks. When increasing the mass velocity, CHF was observed to increase, while the rate of increase was slower at high velocities. CHF showed instead reversed tendency with increasing inlet saturation temperature depending on the flow condition and the channel size.
Ali and Palm [7] analyzed experimental results of dryout during flow boiling in minichannels with internal diameters of 1.22 mm and 1.70 mm. Test were performed at two different saturation temperature of 27 and 32 °C, with mass flux varying from 50 to 600 kg/m^2 s. The authors observed that the dryout heat flux increased with mass flux and decreased with tube diameter, while system pressure had no clear effect for the range of experimental conditions covered.
As it is evident from the literature abovementioned and other researches available [8]-[12], most of the studies concentrate their attention on single-phase flows with water or two-phase flows of refrigerants at saturation temperatures ranging from 20 to 50 °C. In particular, quantitative information about critical heat flux of refrigerants at medium reduced pressures (i.e. reduced temperatures) is still limited.
Recently, concentrated photovoltaic systems allow to work also at solar concentration factors greater than 200 suns, reaching higher heat flux and therefore more electrical power output: in such cases the increase of power is able to compensate for the photovoltaic cell drop in efficiency due to higher working temperatures.
The aim of this study is therefore to carry-out an experimental campaign for the measurement of saturated flow boiling critical heat flux at high reduced pressure conditions in a multi-minichannel aluminum heat sink.

2. Test rig and experimental procedure

An experimental apparatus has been set up in order to investigate the critical heat flux during flow boiling of refrigerants. A schematic diagram of the test facility is shown in Fig. 1.

A. Refrigerant and secondary loop

The refrigerant R134a is pumped in the main loop thanks to a magnetic gear pump (GC – M23JF5S6 Techma gpm), powered by a 0.37kW electrical motor. The pump is able to elaborate volumetric flow rates from 1.3 dm^3/min (at 1650 rpm) up to 2.5 dm^3/min (at 3400 rpm). It is actuated by an inverter which allows a fine regulation of the refrigerant flow rate. A Coriolis effect mass flow meter is installed in the main loop, after the pump, for the measurement of the R134a mass flow rate. Just before entering the test section, an absolute pressure transducer has been inserted in order to measure the inlet system pressure and a resistance thermometer has been included to determine the inlet refrigerant temperature. A differential pressure transducer is used to evaluate the pressure drop in crossing the test section.
At the outlet of the test section, the organic fluid passes through a throttling valve, which can be manually regulated in order to adjust the system mass flow rate and pressure. The refrigerant then enters the condenser, which is a plate heat exchanger, and finally it flows into the liquid receiver and the sub-cooler, that is a double pipe heat exchanger, in order complete the loop.
The main loop is provided with a by-pass line placed right after the pump: in case very small mass flow rates are required, this circuit allows a certain fraction of the entire organic fluid stream to avoid the test section and to flow directly to the liquid receiver.
Demineralised water circulates in the secondary loop. From the suction pipe (see Fig. 1) directly linked to a thermostatic bath, the water passes through the double pipe sub-cooler, the circulation pump (Wilo TOP-S 25/10), the plate heat exchanger and the discharge pipe. Both heat exchangers are provided with a manually-controlled by-pass loop. An expansion vessel guarantees the restraint of variations of specific volume.

B. Test section

The test section is an aluminium heat sink made up of six rectangular fins characterized by a height of 3 mm and a width of 1.85 mm. A photograph of the multi-minichannel heat exchanger is given in Fig. 2. These fins are closed with an aluminium-cogged cover that provides seven minichannels, which are 2.0 mm wide, 1.0 mm deep and 35 mm long. Two manifolds for the inlet and outlet sections were provided, in order to avoid excessive discrepancies in pressure drop and therefore to prevent flow maldistribution. The test section was electrically heated using AC power supply and a ceramic heater (Watlow CER -1-01-00002D) put underneath the channels. This device could provide heating power of 697 W (at ambient temperature) over a base area equal to 2.50x2.50 cm^2, with a nominal base heat flux up to 110 W/cm^2. The electrical power to the test section is provided and regulated by a solid state relay (Gavazzi RM1E40AA25), which is able to achieve an output voltage up to 400 V. A wattmeter, linked between the heater and the solid state relay, is used for the power measurements, whereas four resistance thermometers (RTDs) are equidistantly placed in the test section to evaluate the wall temperature along the minichannels.
The whole test rig has been insulated, with special attention given to the test section. The thermal insulation layer consists of flexible interlaced foam based on synthetic rubber Armaflex IT, supplied by Armacell GmbH, with a thermal conductivity $\lambda < 0.042$ W/m K for the whole range of experimental conditions.

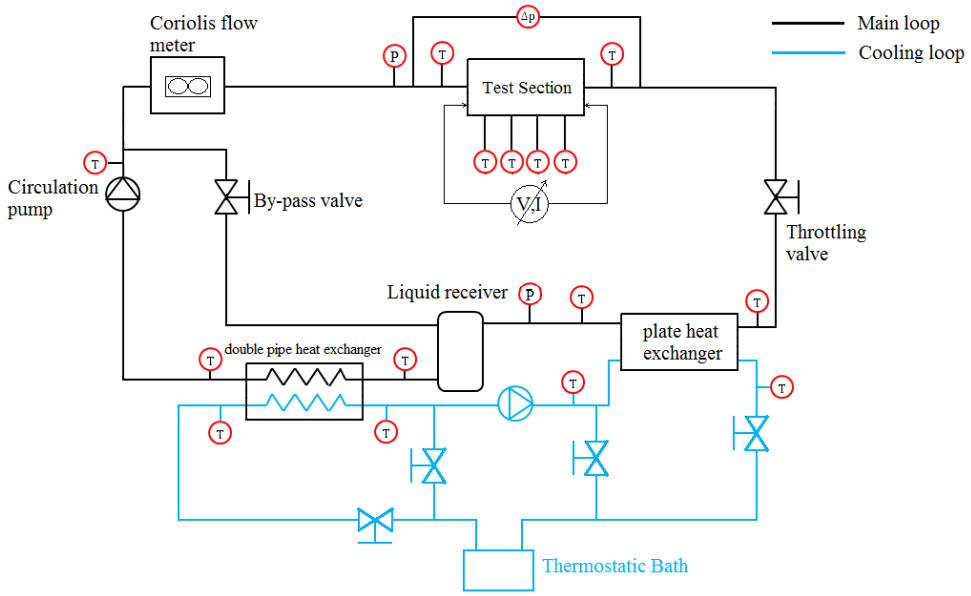

Fig. 1 Simplified schematic diagram of the test facility

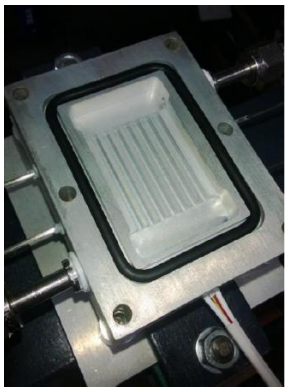

Fig. 2 A view of the multi-minichannel heat sink

C. *Experimental procedure*

The desired test conditions in terms of inlet pressure, inlet temperature (i.e. inlet sub-cooling) and mass flux were kept stable at the beginning of each test. All tests were then performed in steady state conditions.

Specifically, the inlet pressure was commanded by the imposed temperature of the thermostatic bath. Small adjustments could be manually obtained with the throttling valve and the use of the by-pass loop. The inlet temperature was controlled by the opening and closure of the secondary by-pass loop for the double pipe heat exchanger. The refrigerant mass charge in the test facility has however been kept reasonably low not to have high degree of sub-cooling in the whole range of saturation temperatures tested. The required mass flux was finally imposed by changing the inverter frequency of the electric motor coupled with the magnetic gear pump.

The refrigerant entered the test section in sub-cooled liquid and the electrical power was applied in small increments to initiate the boiling mechanism. The system was let to stabilize before the data were recorded. For each condition, tests were performed up to the thermal crisis. During tests, the mass flow rate with increasing heat flux was gradually adjusted with the by-pass valve and/or the throttling valve, in order to re-gain the nominal mass flux chosen for the current experiment. The ceramic heater temperature was constantly monitored with a K-type thermocouple and the power supply was shut-off when it reached the limit of 120 °C, in order not to irreparably damage the test section.

As soon as the system was considered to have reached steady-state conditions, several outputs were read in a fixed interval of time and written into a text file. The default recording time has been manually set to five minutes, with a recording frequency of 1 Hz, resulting in 300 measurements. The nominal value of each data point was assigned to the sample average value. The tests were considered well-steady when the maximum deviation of each value from the measured average did not exceed the 3 %.

All data were saved in Excel files, ready to be used in further processing with the MATLAB software. All thermal and transport properties (including enthalpy, density, viscosity and thermal conductivity) of R134a were calculated using the software REFPROP 9 developed by NIST.

3. Measurement Instrumentation and Data Reduction

A. Measurement instrumentation

All temperature measurements in the test facility are performed with resistance thermometers (Tersid 4-wire Pt100 RTDs). Two RTDs are placed at the inlet and the outlet of the test section and other identical sensors are positioned throughout the main and the secondary loop (see Fig. 1). The sensors are placed right outside the walls and fixed with a nano-aluminium thermal compound (λ = 11.2 W/m K) to guarantee the good equivalence between the fluid and the copper wall temperatures. Their measurement uncertainty is found to be ±0.180 °C. Four 4-wire Pt100 cylindrical RTDs are instead placed inside the test section for the measure of the temperature at heat exchange surface. Their measurement uncertainty results to be ±0.154 °C.

Two absolute pressure transducers (Tersid CTE8050) are placed at the inlet of the test section and at the inlet of the liquid receiver. They are both able to measure pressure in the range 0 – 50 bar. According to the manufacturer, the instrument accuracy, taking into account the non-linearity, hysteresis and repeatability effects, has a typical value of 0.1 %, with a maximum value of 0.3 % (span error). The maximum uncertainty in absolute pressure measurements results to be ±0.188 bar.

Pressure drop in the test section is measured using a differential pressure transducer (Rosemount 2051), with a maximum span error of 0.75 % at full scale, which gives an absolute uncertainty of ±0.45 kPa.

A highly accurate Coriolis flow meter (MicroMotion S12S) has been installed in the main loop to measure the mass flow rates in all test performed. The instrument has been tested up to 115.17 g/s. During calibration, the maximum error was found to be 1 %, resulting in an absolute uncertainty of ±1.15 g/s at full scale.

The wattmeter (HM8115-2) used for the heat power measurements has been tested by the manufacturer. The occurring percent error was found to be 1%, resulting in a maximum uncertainty of ± 10 W at full scale.

As a summary, Tab. 1 shows all the measurement instrumentations used in the experimental test rig and their corresponding uncertainty, by utilizing a coverage factor of k = 1.

Tab.1 Measurement instrumentation and uncertainties

Part numb.	Measurement	Range	Uncertainty (k=1)
Tersid 4-wire Pt100 RTD	Temperature	-	±0.180 °C
Tersid 4-wire Pt100 cylindrical RTD	Temperature	-	±0.154 °C
Tersid CTE8050	Absolute pressure	0 – 50 bar	±0.188 bar
Rosemount 2051	Differential pressure	0 – 60 kPa	±0.45 kPa
MicroMotion S12S	Flow meter	0.00-115.7 g/s	±1 %
HM8115-2 Wattmeter	Electrical power	0-8 kW	±1 %

A. Data Reduction

For a given test point, the base heat flux $\dot{q}_b$ coming from the ceramic heater is calculated as:

$$\dot{q}_b = \frac{\dot{Q}}{A_b} \ [W/cm^2] \quad (1)$$

Where $\dot{Q}$ is the measured heat power and A_b is the ceramic heater base area of 2.50x2.50 cm^2.

The wall heat flux on the channels wall based on the effective heat exchange area must be calculated to reduce data to general terms and compare with prediction methods found in literature. The fin efficiency must be taken into account, using the following equation:

$$\dot{q}_w = \frac{\dot{Q}}{(2 \cdot h_{ch} \cdot \eta + w_{ch}) \cdot N \cdot L_h} \ [W/cm^2] \quad (2)$$

being h_{ch} and w_{ch} the minichannels height and width, respectively, η the fin efficiency, N the number of channels and L_h the heated length. In the present work, for the fin efficiency has been chosen a value of 0.9.

The inlet mass flux has been derived from the measured mass flow rate by taking into account the minichannels cross-sectional area:

$$G = \frac{\dot{m}}{N \cdot w_{ch} \cdot h_{ch}} \ [kg/m^2 s] \quad (3)$$

The inlet sub-cooling has been evaluated by using the measured inlet temperature and the measured inlet pressure, which led to a specific inlet saturation temperature obtained with the software REFPROP.

$$\Delta T_{sub} = T_{sat}(P_{in}) - T_{in} \ [°C] \quad (4)$$

For the computation of the average wall superheat, the following equation has been considered:

$$\overline{\Delta T}_{wall} = \overline{T}_{wall} - T_{sat}(P_{in}) \ [°C] \quad (5)$$

The average wall temperature has been calculated with the arithmetical average of the four RTDs placed inside the test section:

$$\overline{T}_{wall} = \frac{T_{RTD1} + T_{RTD2} + T_{RTD3} + T_{RTD4}}{4} \ [°C] \quad (6)$$

Actually, the real wall temperature is not the one measured by the RTDs installed into the test section. By assuming one-dimensional regime and with the aid of the schematic representation in Fig. 3, the wall temperature results to be:

$$T_{wall} = T_{RTD} - \frac{\dot{q}_w \cdot s_1}{\lambda_{al}} \ [°C] \quad (7)$$

where λ_{al} is the aluminium thermal conductivity, s_1 is the distance between wall heat transfer and the RTD. Even with the highest heat flux imposable, the subtractive term is considerably negligible and thus the wall temperature

might be correctly obtained with the sensors' measurements:

$$T_{wall} \cong T_{RTD} \quad (8)$$

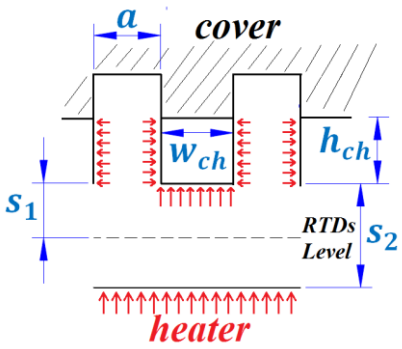

Fig. 3 Channel geometry

4. Experimental results

The results have been given in form of boiling curves from which the critical heat flux has been deduced. Since the thermal crisis was not always evident as a sudden flat deviation from the boiling curve trend, the critical heat flux for all the experiments performed has been defined as the heat flux at which the boiling curve decreases its slope $\Delta q/\Delta T$ below a limit value, following the same approach of Mauro et al. [2]. In this work, the gradient indicating the onset of CHF was chosen to be 2.5 W/K cm^2.

Tests were performed with R134a at several high saturation temperatures, from 25°C up to 70 °C, with mass fluxes ranging from 150 to 330 kg/m^{2}s and inlet sub-cooling-from 6 to 10 K.

The parametric effects of mass flux and saturation temperature were investigated. The inlet sub-cooling effect was not taken into account since it has seen that except for high values (e.g. 20 K), it has a minor role, especially for narrow channels [6].

The effects of mass velocity on CHF are shown in Fig. 4, which displays four boiling curves at T_{sat} = 70 °C and at four mass fluxes equal to 149, 215, 288 and 330 kg/m^2 s.

It can be seen that when increasing the mass velocity at a fixed saturation pressure, CHF increases significantly, passing from 43 W/cm^2 up to 84 W/cm^2 for the highest mass flux imposed. The first parts of the boiling curves follow the same points, indicating that the mass flux has almost no influence on the boiling heat transfer coefficient and hence the boiling phenomenon is controlled by the nucleate mechanism.

The effect of saturation temperature (i.e. system pressure) is depicted in Fig. 5, which shows six boiling curves at G = 210 kg/m^2 s and at six saturation temperatures equal to 25, 33, 46, 53, 64, 70 °C. The system pressure seems to give only a slight effect on CHF, since all the curves' slopes are dropping when heat flux reaches approximately 70 W/cm^2. Also in this case, the remarkable effect of the saturation pressure on the boiling curves' slope indicates that the nucleate boiling mechanism seems to dominate before thermal crisis occurs.

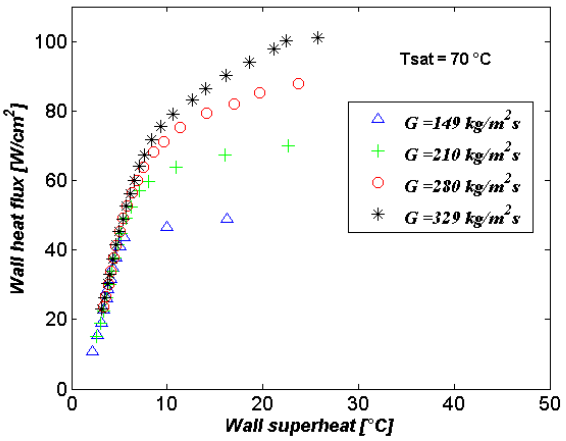

Fig. 4 Boiling curves with T_{sat} = 70 °C and different mass fluxes G equal to: 149, 210, 280 and 329 kg/m^2 s.

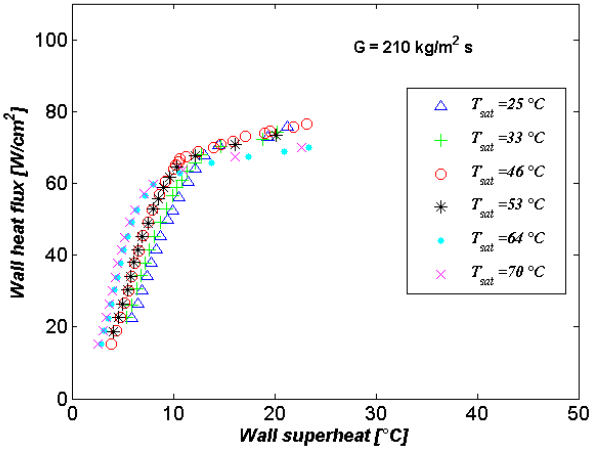

Fig. 5 Boiling curves with G = 210 kg/m^2 s and different saturation temperatures T_{sat} equal to: 25, 33, 46, 53, 64 and 70 °C

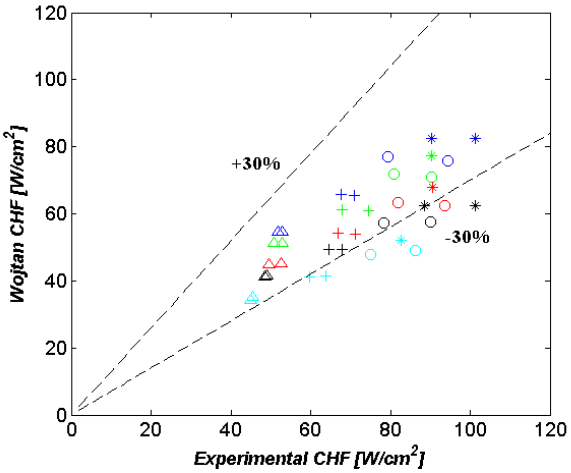

Fig. 6 Comparison of Wojtan et al. correlation with present data

The experimental CHF values are finally compared with the well-known correlation of Wojtan et al. [4], expressly developed for R134a and R245fa in minichannels. In Fig. 6, the estimate Wojtan et al. CHFs are plotted against the experimental points. The Mean Absolute Deviation

(MAD) has been used to compare the experimental CHF data with the Wojtan correlation from literature. MAD is given by:

$$\boldsymbol{MAD} = \frac{\mathbf{1}}{\boldsymbol{n}} \sum_{\boldsymbol{i}=\mathbf{1}}^{\boldsymbol{n}} \left| \frac{\dot{q}_{CHF,pred} - \dot{q}_{CHF,exp}}{\dot{q}_{CHF,exp}} \right| \cdot \mathbf{100} \qquad (9)$$

This correlation predicts the experimental data with a MAD of 8.9 %. The highest errors are found in tests performed with high saturation temperatures, for which the effectiveness of the abovementioned correlation has not been guaranteed by the authors.

5. Conclusions

The current work presents a series of experiments in order to investigate the critical heat flux (CHF) characteristics during flow boiling of R134a in an aluminium multi-minichannel heat sink. The influence of mass flux and system pressure has been discussed in the paper and the experimental data are compared with the predictions of Wojtan et al. correlation. Specifically, the main outcomes of this study are:

- The mass flux has a strong influence on the CHF, meaning that at increasing mass velocities, the critical values are increasing as well.
- The saturation temperature has a negligible influence on the CHF. The critical heat flux seems to slightly decrease with increasing system pressure, but this behaviour was not found to be systematic.
- The boiling process is mainly controlled by nucleate boiling: mass velocity has not a considerable effect on the boiling curves' slope, whereas the increase in saturation temperature, leads to a lower wall superheat and therefore a higher heat transfer efficiency.
- The correlation of Wojtan et al. slightly underestimates most of the experimental data. However, the calculated MAD of 8.9 % is very low and the largest deviations are obtained for high saturation temperatures, out of the formula operative conditions range.

Further research in this field is still needed to fully understand the behaviour of compact heat sinks with high thermal duties. For instance, the influence of the minichannel geometry has not been investigated in this work, as well as the influence of the working fluid. It might be also useful to use different heated lengths and to allow flow visualization, in order to better associate the flow patterns to dryout phenomena.

References

[1] Royne A., Dey C.J., Mills D.R., Cooling of photovoltaic cells under concentrated illumination: a critical review. Solar Energy Materials and Solar Cells 84 (2005), pp. 451-483.

[2] Mauro A.W. , Thome J.R., Toto D., Vanoli G.P, Saturated critical heat flux in a multi-microchannel heat sink fed by a split flow system. Experimental Thermal and Fluid Science 34 (2010), pp. 81-92.

[3] Lazarek G.M., Black S.H., Evaporative heat transfer, pressure drop and critical heat flux in a small vertical tube with R-113. Int. J. of Heat and Mass Transfer 25 (1982), pp. 945-960.

[4] Wojtan L., Revellin R., Thome J.R., Investigation of saturated critical heat flux in a single, uniformly heated microchannel. Experimental Thermal and Fluid Science 30 (2006), pp. 765–774.

[5] Tibiriçá C., Ribatsk G., Thome J.R., Saturated flow boiling heat transfer and critical heat flux in small horizontal flattened tubes. Int. J. of Heat and Mass Transfer 55 (2012), pp. 7873-7883.

[6] Park J.E., Thome J.R., Critical heat flux in multi-microchannel copper elements with low pressure refrigerants. Int. J. of Heat and Mass Transfer 53 (2010), pp. 110-122.

[7] Ali R., Palm B., Dryout characteristics during flow boiling of R134a in vertical circular minichannels. Int. J. of Heat and Mass Transfer 54 (2011), pp. 2434-2445.

[8] Bowers M.B., Mudawar I., High flux boiling in low flow rate, low pressure drop mini-channel and micro-channel heat sinks. Int. J. of Heat and Mass Transfer 37 (1994), 321-332.

[9] Agostini B., Revellin R., Thome J.R., Fabbri M., Michel B., Calmi D., Kloter U., High heat flux flow boiling in silicon multi-microchannels: Part III – saturated critical heat flux of R236fa and two-phase pressure drops. Int. J. of Heat and Mass Transfer 51 (2008), pp. 5426-5442.

[10] Martin-Callizo C., Ali R., Palm B., Dry-out incipience and critical heat flux in saturated flow boiling of refrigerants in a vertical uniformly heated microchannel. In: Proceedings of the 6th International Conference on Nanochannels, Microchannels, and Minichannels. Darmstadt, Germany, June 23–25, 2008.

[11] Maqbool M.H., Flow boiling of ammonia and propane in mini channels. Doctoral Thesis. Division of Applied Thermodynamics and Refrigeration Department of Energy Technology, Royal Institute of Technology, (KTH) Stockholm, Sweden 2012.

[12] Owhaib W., Experimental Heat Transfer, Pressure Drop, and Flow Visualization of R-134a in Vertical Mini/Micro Tubes. Doctoral Thesis. Division of Applied Thermodynamics and Refrigeration Department of Energy Technology, Royal Institute of Technology, (KTH) Stockholm, Sweden 2007.